Chapter 2

Background

In this chapter gives the overviews of the piezoelectric pyroelectric and diffusivity phenomenon, together with the way to obtain these properties. This chapter also includes a description of composite materials.

1. Piezoelectricity

1.1 History of the Piezoelectricity

The Curie brothers, Pierre and Jacques first discovered the physical piezoelectric effect in 1880. Their experiment consisted of a conclusive measurement of surface charges appearing on specially prepared crystals (tourmaline, quartz, topaz, cane sugar and Rochelle salt) which were subjected to mechanical stress. This was the direct piezoelectric effect. The existence of an inverse piezoelectric effect was mathematically deduced from fundamental thermodynamic principles by Lippmann in 1881. Soon thereafter the converse effect, the geometrical strain of a crystal proportional to an applied voltage was shown. During the years following the discovery of the piezoelectric effect, several well known researchers, including Lord Kelvin, Pockels and Dusem developed the theory of the piezoelectricity (Cady, 1964) .

After only two years of interactive work within the European scientific community, the core of piezoelectric applications science was established: the identification of piezoelectric crystals on the basis of asymmetric crystal structure, the reversible exchange of electric and mechanical energy, and the usefulness of thermodynamics in quantifying complex relationships among mechanical variables (Jaffe et al.,1985).

In the following 25 years (leading up to 1910), much more work was done to make this core grow into a versatile and complete framework which defined

completely the 20 natural crystal classes in which the piezoelectric effects occur. In 1910, the state of piezoelectric knowledge was summarized in "Lerbuch der Kristallphysikk" by Voigt and first published in Berlin (Cady, 1964).

The first serious applications work on piezoelectric devices took place during World War I. In 1917, P. Langevin and French co-workers made an ultrasonic submarine detector, composing of thin quartz crystals glued between two steel plates. They achieved their goal of emitting a high frequency "chirp" underwater and measuring depth by timing the return echo. The strategic importance of their achievement was not overlooked by any industrial nations, however, since that time the development of sonar transducers, circuits, systems, and materials has never ceased. Most of the classic piezoelectric applications with which we are now familiar are, for example, microphones, loudspeakers, accelerometers, ultrasonic transducers, bender element actuators, phonograph pick-ups, signal filter, etc.

During World War II, in the U.S., Japan and the Soviet Union, isolated research groups working on improved capacitor materials discovered that certain ceramic material (prepared by sintering metallic oxide powders) exhibited dielectric constants up to 100 times higher than common cut crystals.

The advances in materials science that were made during this phase fall into three categories:

1. Development of the barium titanate family of piezoceramics and later the lead zirconate titanate family
2. The development of an understanding of the correspondence of the perovskite crystal structure to electro-mechanical activity
3. The development of a rationale for doping both of these families with metallic impurities in order to achieve desired properties such as dielectric constant, stiffness, piezoelectric coupling coefficients, ease of poling, etc.

All of these advantages contributed to establishing an entirely new method of piezoelectric device development-namely, tailoring a material to a specific application, as follows:

- Powerful sonar-based on new transducer geometries (such as spheres and cylinders) and sizes achieved with ceramic casting.
- Ceramic phono cartridge-cheap, high signal elements simplified circuit design.
- Piezo ignition systems-single cylinder engine ignition systems which generated spark voltages by compressing a ceramic "pill".
- Sonobouy-sensitive hydrophone listening/radio transmitting bouys for monitoring ocean vessel movement.
- Microphones-became small and sensitive.
- Ceramic audio tone transducer-small, low power, low voltage, audio tone transducer consisting of a disc of ceramic laminated to a disc of metal sheet.
- Relays-snap action relays were constructed and studied.

The search for perfect piezo product opportunities is now in progress judging from the increase in worldwide activity, and from the successes encountered in the last quarter of the 20th century (Setter, 2002).

1.2 Piezoelectric effect

The relation between the electric displacement (D), electric field (E) and polarization (P) in a dielectric material is defined as:

$$D = \varepsilon_0 E + P \tag{2.1}$$

where ε_0 is the permittivity of free space = 8.854×10^{-12} F/m. The polarization expressed by following relationship:

$$P = \varepsilon_0 \chi E \tag{2.2}$$

where χ is the electric susceptibility. By equation (2.2), equation (2.1) can be rewritten as:

$$D = \varepsilon_0(1+\chi)E \tag{2.3}$$

According to ε_r is relative permittivity or dielectric constant, ε is the permittivity of the material and

$$D = \varepsilon_0\varepsilon_r E = \varepsilon E \tag{2.4}$$

The polarization of the dielectric material is influenced by the stress (σ) exerted on it through the direct piezoelectric effect, by the electric field applied to it through the inverse piezoelectric effect, and temperature changes (ΔT) through the pyroelectric effect as shown in equation (2.5).

$$D = p^{\sigma}\Delta T + d^{T}\sigma + \varepsilon^{T,\sigma}E \tag{2.5}$$

where p is the pyroelectric coefficient and d is the piezoelectric coefficient. Similarly, the strain (S) of the material is influenced by the temperature changes through the thermal expansion (γ), by the applied electric field through the converse piezoelectric effect, and by the stress:

$$S = \gamma^{E}\Delta T + d^{T}E + s^{T,E}\sigma \tag{2.6}$$

where s^E is the elastic compliance. The superscripts denote the parameter held constant.

When a stress is applied to dielectric materials, they develop an electric moment whose magnitude is proportional to the applied stress. Conversely, if an electric field is applied to the materials, the mechanical distortion will produce in those materials. The reciprocal relationship is referred to as *the piezoelectric effect*. The phenomenon of generation of a voltage under mechanical stress is referred to as *the direct piezoelectric effect*, and the mechanical strain produced in the crystal under electric field is called *the converse piezoelectric effect*. The necessary condition for the piezoelectric effect is the absence of a center of symmetry in the crystal structure. The

32 crystal classes 21 lack a center of symmetry, and with the exception of one class (cubic 432), all of these are piezoelectric (see Table 2.3). Figure 2.1 shows a simple illustration the piezoelectric effect. The relationships between the mechanical variation and electrical variation in the piezoelectric effect are:

$$D = d\sigma + \varepsilon^{\sigma} E \qquad \text{direct piezoelectric effect} \qquad (2.7)$$

$$S = s^{E}\sigma + dE \qquad \text{converse piezoelectric effect} \qquad (2.8)$$

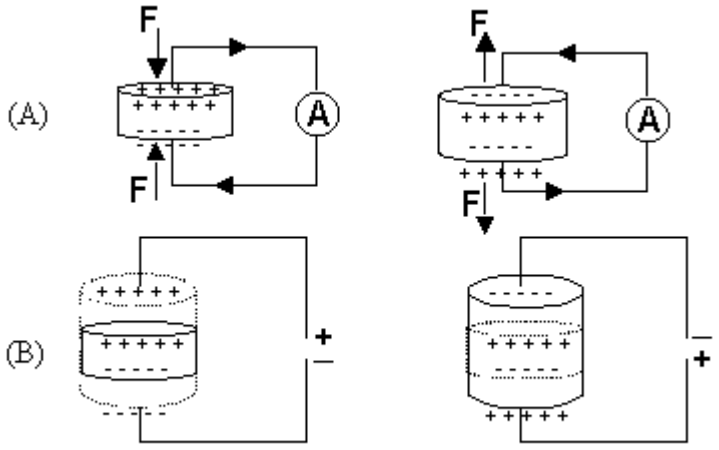

Figure 2.1 Illustration of A) direct and B) converse piezoelectric effect for a material with a positive value of *d* coefficient

The piezoelectric components depend on the boundary conditions in which the element is placed. If the element is short-circuited, $E = 0$, then equation (2.7) becomes

$$D = d\sigma \qquad (2.9)$$

This gives a definition of the important constant *d*, the piezoelectric charge constant, which is defined as the dielectric displacement developed per unit applied mechanical stress at constant electric field.

The dual definition of *d* is obtained by considering the element operating in a no-load condition ($\sigma = 0$) so that equation (2.8) becomes:

$$S = dE \tag{2.10}$$

Therefore a second definition for the constant *d*, the piezoelectric strain constant, is the mechanical strain produced per unit applied field at the constant external stress. When there is no piezoelectric effect (*d*=0) then equation (2.7) and (2.8) simplify to the well known relationships:

$$s^E = \frac{S}{\sigma} = elastic\ compliance \tag{2.11}$$

$$\varepsilon^\sigma = \frac{D}{E} = electrical\ permittivity \tag{2.12}$$

Both equation (2.11) and (2.12) are valid, if either *E* or σ is zero.

In equation (2.7) and (2.8) the chosen independent electrical and mechanical variables were the electric field and the mechanical stress. Other independent variables can be chosen as well. If the electrical displacement and mechanical stress are chosen as variables, the constitutive equations can be obtained by the following analysis.

When *D* = 0 (open-circuited element), equation (2.7) becomes

$$E = -\frac{d}{\varepsilon^\sigma}\sigma \tag{2.13}$$

$$\text{if} \quad g = \frac{d}{\varepsilon^\sigma}, \qquad E = -g\sigma \tag{2.14}$$

Equation (2.8) can be rewritten as

$$E = -g\sigma + \frac{D}{\varepsilon^\sigma} \tag{2.15}$$

Thus *g*, the piezoelectric voltage constant, is defined as the field developed per unit applied mechanical stress (direct piezoelectric effect) under open circuit conditions. From equation (2.12), equation (2.10) can be expressed as

$$S = d\frac{D}{\varepsilon^{\sigma}} \tag{2.16}$$

$$\text{if} \quad g = \frac{d}{\varepsilon^{\sigma}} \qquad S = gD \tag{2.17}$$

Equation (2.8) can be rewritten as

$$S = s^{E}\sigma + (g\varepsilon^{\sigma})E \tag{2.18}$$

From equation (2.12), $D = \varepsilon^{\sigma}E$, equation (2.20) becomes:

$$S = s^{E}\sigma + gD \tag{2.19}$$

An alternative definition for *g* is the strain obtained per unit applied electric displacement at constant external stress. The '*g*' coefficient is useful when the voltage response to an applied stress is of concern. While the '*d*' coefficients are of interest in low frequency applications, another set of coefficients is useful at high frequency or under mechanically clamped conditions (*S*=0). In the latter cases the constitutive equations are:

$$D = eS + \varepsilon^{s}E \tag{2.20}$$

$$\sigma = c^{E}S - eE \tag{2.21}$$

where *c* is the stiffness. The '*e'* coefficients is related to the '*d*' coefficients by:

$$e = dc \tag{2.22}$$

Finally, the clamped voltage '*h*' coefficient can be derived from the constitutive equations when the independent variables are the strain and electric displacement:

$$E = -hS + \frac{D}{\varepsilon^s} \tag{2.23}$$

$$\sigma = c^D S - hD \tag{2.24}$$

The '*h*' coefficient is related to the '*e*' coefficient by:

$$h = \frac{e}{\varepsilon} \tag{2.25}$$

Table 2.1 collects the constitutive relations of each pair of chosen independent variables. From the table, *d* and *g* are "*the piezoelectric strain coefficient*" and *e* and *h* are "*the piezoelectric stress coefficient*".

Table 2.1 Piezoelectric coefficients

Piezoelectric coefficient	Definition	
d $(E,\ \sigma)$	$\frac{dielectric\ displacement\ developed\ (D)}{applied\ mechanical\ stress\ (\sigma)}$	$(E = constant)$
	$\frac{strain\ developed(S)}{applied\ field(E)}$	$(\sigma = constant)$
g (D,σ)	$\frac{field\ developed(E)}{applied\ mechanical\ stress(\sigma)}$	$(D = constant)$
	$\frac{strain\ developed(S)}{applied\ dielectric\ displacement(D)}$	$(\sigma = constant)$

Table 2.1 (continued) Piezoelectric coefficients

Piezoelectric coefficient	Definition	
e (E, S)	$\frac{dielectric\ displacement\ developed(D)}{applied\ strain(S)}$	($E = constant$)
	$\frac{stress\ developed(\sigma)}{applied\ field(E)}$	($S = constant$)
h (D, S)	$\frac{field\ developed(E)}{applied\ strain(S)}$	($D = constant$)
	$\frac{stress\ developed(\sigma)}{applied\ dielectric\ displacement(D)}$	($S = constant$)

The combinations of the elastic variables (stress, strain) and dielectric variables (dielectric displacement, electric field) defining four coefficients *d, g, e,* and *h* indicate in Figure 2.2

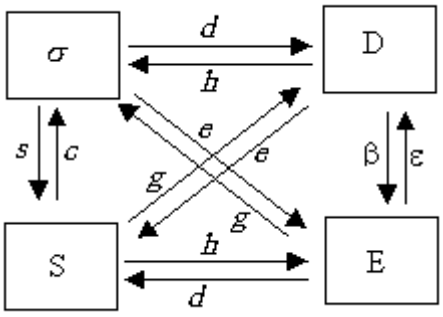

Figure 2.2 Definition of the piezoelectric coefficients

The piezoelectric coefficient is a cross coupling between the elastic variables (σ, *S*) and the electric variables (*D*, *E* and *P*). Since the elastic variables are second-

rank tensors with nine components and the electric variables are vectors which are specific by three components. So the piezoelectric coefficients are third-rank tensors with 27 components. Equation (2.7) and (2.8) in full tensor notation become equation (2.26) and (2.27), respectively.

$$D_i = d_{ijk}\sigma_{jk} \tag{2.26}$$

$$S_{jk} = d_{ijk}E_i \qquad i,j,k = 1,2,3 \tag{2.27}$$

Since d_{ijk} is symmetrical in j and k ($d_{ijk} = d_{ikj}$), the number of independence elements of the piezoelectric coefficients can be reduced to 18 components. Simplified matrix notation often replaces the tensor notations. Table 2.2 summarizes these notations for the piezoelectric coefficient (d), and other relevant properties.

Table 2.2 Tensorial properties expressed in matrix notation (Setter, 2002).

Tensor notation	Matrix notation
11	1
22	2
33	3
23,32	4
13,31	5
12,21	6
σ_{ij} ; *when* $i = j$	σ_p ; p =1,2,3
σ_{ij} ; *when* $i \neq j$	σ_p ; p =4,5,6
S_{ij} ; *when* $i = j$	S_p ; p =1,2,3
S_{ij} ; *when* $i \neq j$	$\frac{1}{2}S_p$; p =4,5,6
d_{ijk} ; *when* $i = j$	d_{ip} ; p =1,2,3
d_{ijk} ; *when* $i \neq j$	$\frac{1}{2}d_{ip}$; p =4,5,6

The physical significance of the subscripts used in the matrix notation is shown in Figure 2.3.

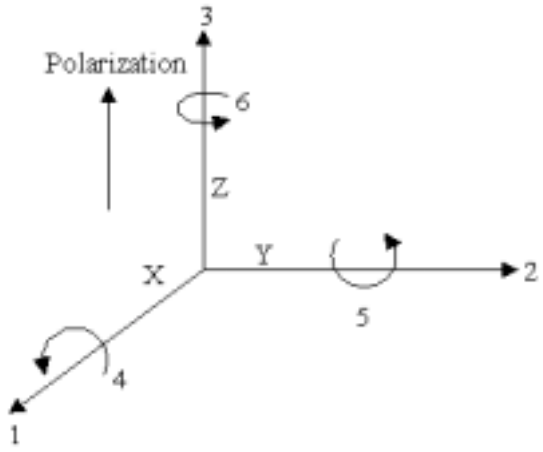

4 = shear in 23 plane, 5 = shear in 31 plane and 6 = shear in 12 plane

Figure 2.3 Illustration of the direction associated with the subscripts used in the matrix notation.

Equation (2.26), (2.27) can be rewritten in the matrix notation as:

$$D_i = d_{ij}\sigma_j \tag{2.28}$$

$$S_j = d_{ij}E_i \qquad i=1,2,3 \text{ and } j= 1,2,3\ldots,6 \tag{2.29}$$

Equation (2.29) is the main equation for piezoelectric measurements in the present work. In practice, the first subscript i of d_{ij} is refer that the electric field is applied in the i axis. The second one is refer that the strain generating in the j axis.

Applying the appropriate piezoelectric and elastic coefficients for the conversion of mechanical energy (stress times strain) into electrical energy (displacement times electric field) gives the relation:

$$k^2 = \frac{d^2}{s^E \varepsilon^T} \tag{2.30}$$

1.3 Piezoelectric coefficient measurements

1.3.1 Static and quasi-static methods

The earliest piezoelectric measurement of the crystals is made by direct measuring piezoelectric effects of static methods. It is made by putting a weight on a crystal and observing the charge generated by some charge detector such as a quadrant electrometer. Due to small the generated electrical charge, part of the electrical charge can leak off before the electrometer can be activated. Hence the direct measuring for the direct effect is usually not reliable.

This method is modified by applying a sinusoidal stress to the crystal and measured the electrical charge (Q) generating as a voltage over a capacitor (C) in a parallel with the crystal (Figure 2.4). The capacitor has a capacitance much larger than the sample to fulfill the free-field condition. The d_{33} can be calculated from

$$d_{33} = \frac{D_3}{\sigma_3} = \frac{Q}{F} = \frac{CV}{F} \tag{2.31}$$

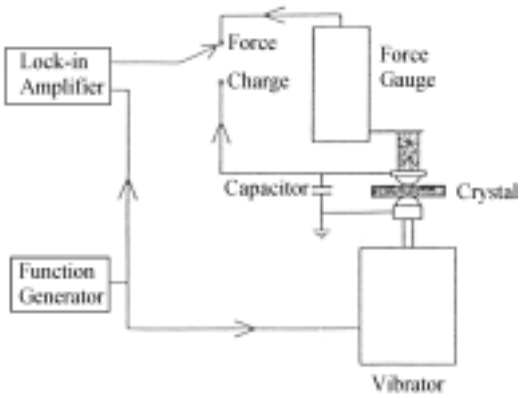

Figure 2.4 Schematic diagram of the setup for measuring the piezoelectric coefficient using the direct piezoelectric effect (Taunaumang and Guy, 1994)

1.3.2 Resonance methods

When exposed to an AC electric field, a piezoelectric ceramic element changes dimensions cyclically, at the cycling frequency of the field. The frequency at which the ceramic element vibrates most readily, and most efficiently converts the electrical energy input into mechanical energy, is the *resonance frequency*. The pattern of an element's response is predicted in Figure 2.5. The composition of the dielectric material and the shape and volume of the element determine the resonance frequency generally, a thicker element has a lower resonance frequency than a thinner element of the same shape. As the frequency of cycling is increased, the element's oscillations first approach a frequency at which impedance is minimum (maximum admittance). The minimum impedance frequency also is the *resonance frequency*, f_r. As the cycling frequency is further increased, impedance increases to a maximum (minimum admittance). The maximum impedance frequency also is the *anti-resonance frequency*, f_a.

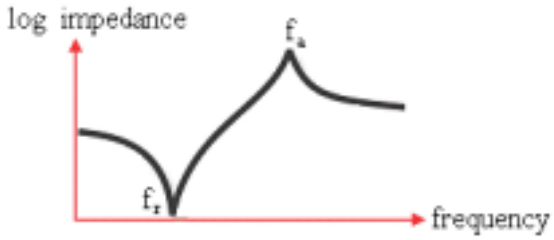

Figure 2.5 Schematic impedance diagram in the frequency region of the piezoelectric resonance

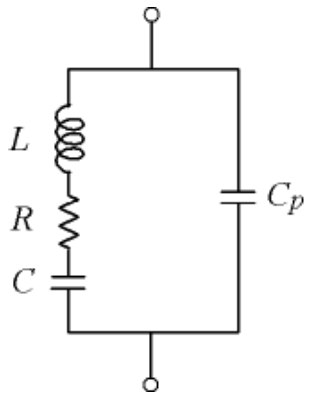

Figure 2.6 Equivalent circuit of a piezoelectric resonator (Mason, 1954)

f_r and f_a can be used to calculate the electromechanical coupling factor ,k. The factor k depends on the mode of vibration and the shape of the ceramic element. A relationship between k, f_r and f_a for a ceramic plate, a disc (surface dimensions large, relative to the thickness), or a rod are (Katiyar and Srivastava, 1994):

$$k_p^2 = \frac{2.51(f_a - f_r)}{f_a} - \left(\frac{f_a - f_r}{f_a} \right)^2 \tag{2.32}$$

$$k_{33} = \left(\frac{\pi}{2} \right) \left(\frac{f_a}{f_r} \right) \tan \left[\left(\frac{\pi}{2} \right) \left(\frac{f_a - f_r}{f_a} \right) \right] \tag{2.33}$$

$$k_{33}^2 = \frac{d_{33}^2}{s^E \varepsilon^T} \tag{2.34}$$

1.3.3 Interferometric technique

The basic principle of the laser interferometer is, for a monochromatic light of wavelength λ interferes with a reference beam, the interference light intensity at the detection point (I). (Zhang, 1988)

$$I = I_1 + I_2 + 2\sqrt{I_1 I_2} \cos \left(\frac{4\pi \Delta d}{\lambda} \right) \tag{2.35}$$

where I_1 ,and I_2 are the light intensity probing beam and reference beam respectively, Δd is optical path-length difference between two beams and λ is wavelength of the laser. A relative change Δd between the two beams resulting in changing the interference light intensity can be detected. Equation (2.35) can thus be written as:

$$I = \frac{1}{2}(I_{\max} + I_{\min}) + \frac{1}{2}(I_{\max} - I_{\min}) \cos(\frac{4\pi \Delta d}{\lambda}) \tag{2.36}$$

From equation (2.36), the maximum change in intensity occurs when $\cos(\frac{4\pi\Delta d}{\lambda}) = 0$. The corresponding Δd is:

$$\Delta d = \frac{1}{2}(2n+1)\frac{\lambda}{4} \qquad \text{where } n = 0,1,2,3,\ldots. \quad (2.37)$$

The situation description of equation (2.37) is often referred to as the $\frac{\lambda}{4}$ condition. The intensity at the center of the interference pattern from interferometer plot as a function of path-length difference shows in Figure 2.8

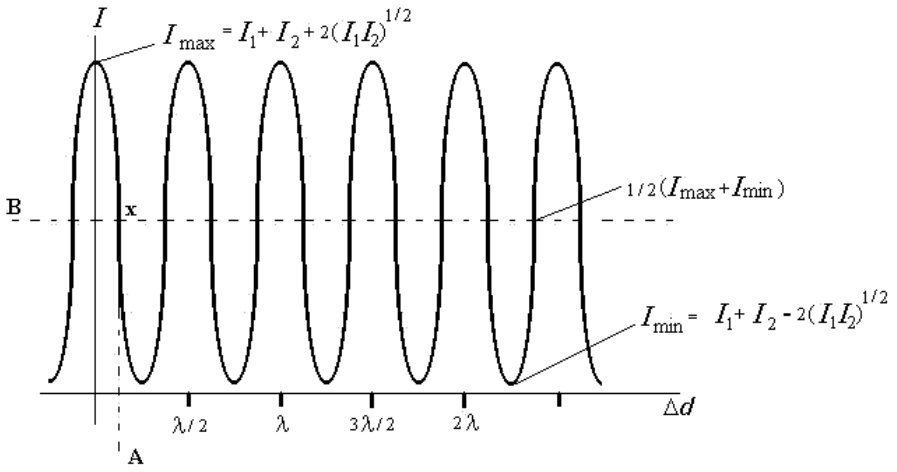

Figure 2.7 The intensity at the centre of the interference pattern from interferometer plot as a function of path-length difference. The labeled X point corresponds to $\frac{\lambda}{4}$ condition.

An AC voltage applied across the sample produces the piezoelectric strain. The strain in the sample produces a small movement of the sample's reflecting surface as shows in Figure 2.8 The small changes in intensity at the detector induced by the sample surface movement are proportional to the surface movement. The changes were measured using a lock-in amplifier connected to detector. The piezoelectric coefficient is the ratio of the strain and the magnitude of applied voltage.

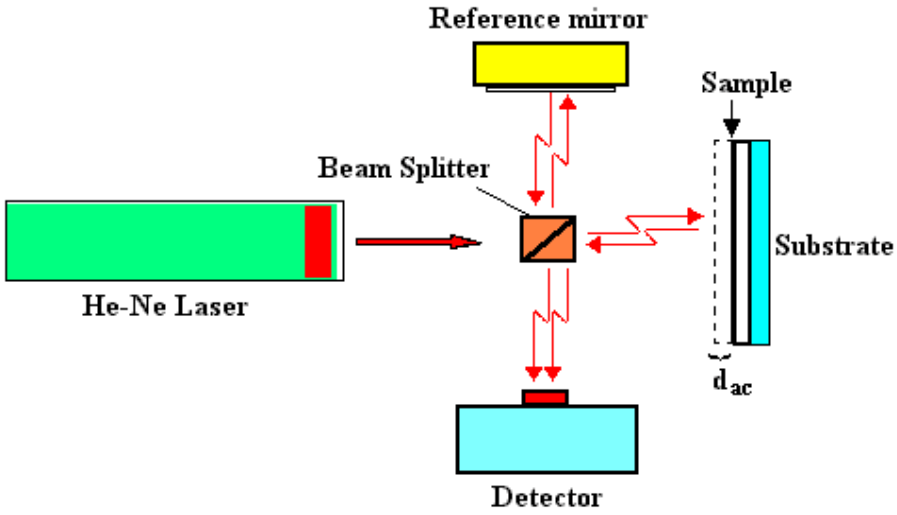

Figure 2.8 The sample displacement caused by an external electric field.

According to equation (2.37), Δd can be rewritten as:

$$\Delta d = d_{ac} + \frac{1}{2}(2n+1)\frac{\lambda}{4} \tag{2.38}$$

where the d_{ac} is a small displacement of the sample surface. From equations (2.35) and (2.36), equation 2.36 can be rewritten as:

$$I = \frac{1}{2}(I_{\max} + I_{\min}) - \frac{1}{2}(I_{\max} - I_{\min})\sin(\frac{4\pi d_{ac}}{\lambda}) \tag{2.39}$$

and $$I = \frac{1}{2}(I_{\max} + I_{\min}) - \frac{1}{2}(I_{\max} - I_{\min})(\frac{4\pi d_{ac}}{\lambda}) \qquad \text{for small } d_{ac} \tag{2.40}$$

Experimentally, the light intensity (I) is measured by a photodetector, which convert photocurrent to a corresponding voltage. The voltage is observed and measured with an oscilloscope. Hence, at a certain gain, the relationship between the photovoltage and the light intensity may be expressed as

$$V = constant \times I \tag{2.41}$$

Consequently, equation (2.61) can be written in terms of measured voltage as follows,

$$V = \frac{1}{2}(V_{\max} + V_{\min}) - \frac{1}{2}(V_{\max} - V_{\min})(\frac{4\pi d_{ac}}{\lambda})) \tag{2.42}$$

A root-mean-square (r.m.s) value of the electrical output V is detected by a lock-in amplifier as V_{out}. Since the lock-in amplifier will only detect the AC component of the signal, the (V_{max}+V_{min}) DC component does not contribute to the output reading. The lock-in detection scheme provides excellent noise rejection. It can be used as the key to an improved sensitive. Therefore, it can be shown that

$$V_{out} = (\frac{2\pi}{\lambda})V_{p-p}\left|d_{ac}\right| \tag{2.43}$$

where $V_{p\text{-}p}$ is the peak-to-peak voltage value of the interference signal, which is equal to (V_{max}-V_{min}) and corresponds to the interference signal changing (I_{max}-I_{min}). By making use of equation (2.43), the piezoelectric coefficient d_{ii} is defined as:

$$d_{ii} = \frac{\lambda V_{out}}{2\pi V_{p-p} V} \tag{2.44}$$

where V is a driving voltage.

2. Pyroelectricity

2.1 Pyroelectric history

The Greek philosopher, Theophrastus, who lived in the fourth century BC, probably wrote the earliest description of the pyroelectric effect, observed in the mineral tourmaline. Two thousand years after Theophrastus, the first serious scientific study of the electrical properties of tourmaline was presented to the Royal Academy of Sciences in Berlin by Franz Theodor Aepinus in 1756. His major observations were tourmaline became electrified by being warmed and the crystal acquired opposite electrical charges on two opposing faces. The usefulness of this new way of generating electrical charges and relevance to the rapidly developing understanding of electricity and magnetism induced many others to experiment on tourmaline. Canton was apparently the first person to observe that cooling of tourmaline caused its electrical polarity to be reversed that found in heating. He also devised a very novel experiment for demonstrating the quantities of positive and negative charge were equal.

During the 19^{th} Century, research in pyroelectricity began to be quantitative. As electrical measuring techniques of higher sophistication were developed and applied to the pyroelectric studies.

In 1859, Jean-Mothee Gaugain made the first very precise measurements of the pyroelectric charge. He reached some important conclusions:

- The total quantity of electricity produced by a crystal of tourmaline depends uniquely upon the limits within which its temperature is varied.
- With in the same temperature limits, the quantity of electricity produced during heating is the same as that produced during cooling, but the sign of the charges are reversed.
- The quantity of charge produced is proportional to the cross-section area of the crystal and is independent of its length.

Jacques and Pierre Curie speculated that the electrical effects due to non-uniform heating of crystals might have been caused by pressure. This instead lead to their discovery of piezoelectricity in 1880.

Matossi experimented on tourmaline detectors at the University of Graz, Austria, during World War II. In 1992, Copper made the first detailed analysis of a fast IR detector and conducted experiments using $BaTiO_3$. In the same year, Lang proposed that use of pyroelectric devices for measuring temperature changes as small as 0.2 μK. An explosive growth in theoretical studies, basic measurements and applications began, culminating in the total of more than 7,000 publications during period 1960-1996.

2.2 Pyroelectric effect

Pyroelectricity refers to the generation of electric charge resulting from temperature change in crystalline materials. A change in temperature will alter the ionic and electronic force within the crystal cell, resulted changing in the dipole moments for polar materials. Since the unit cells of the crystal are aligned, a net change in crystal polarization occurs. This polarization change results changing the surface bound charge density (Figure 2.9). If the crystal is left exposed to the air for sufficiently long time, then the additional bound charges will be compensated by free charges from the surroundings, hence, the changes in crystal polarization will not apparent. If the change in temperature is fast enough then there is no time for charge compensation to occur. The result is that a pyroelectric current will flow in circuit connected to electrodes placed on opposite surfaces of the material.

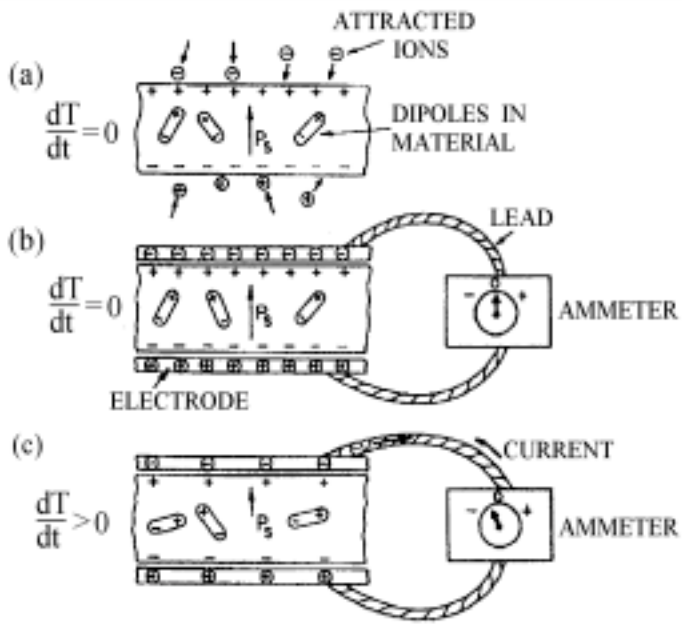

Figure 2.9 Illustration of the pyroelectric effect

The pyroelectric coefficient is defined as the ratio of changing polarization to the temperature change:

$$p = \frac{\Delta P}{\Delta T} \tag{2.45}$$

The electric charge appearing on the electrode of area A is:

$$\Delta Q = (\Delta P)A = (p\Delta T)A \tag{2.46}$$

$$p = \frac{(\Delta Q / A)}{\Delta T} \tag{2.47}$$

Where
p = Pyrorelectric coefficient

ΔP = Polarization change

ΔQ = Electric charge change

ΔT = Temperature change

A = Electrode area

The seven crystal systems, i.e. triclinic (the least symmetrical), monoclinic, orthorhombic, tetragonal, hexagonal and cubic, can be subdivided into thirty-two point groups (crystal class), according to their symmetry with respect to a point. Table 2.3 provides the detail of these point groups arranged by seven crystal systems.

Table 2.3 The 32 crystallographic point groups arranged by crystal systems (Lang and Gupta, 2000).

Crystal system	Symbol	Pyroelectric	Piezoelectric	Centro-symmetry
Triclinic	1	√	√	
	$\bar{1}$			√
Tetragonal	4	√	√	
	$\bar{4}$		√	
	4/m			√
	422		√	
	4mm	√	√	
	$\bar{4}$ 2m		√	
	4/mmm			√
Hexagonal	6	√	√	
	$\bar{6}$		√	
	6/m			√
	622		√	
	6mm	√	√	
	$\bar{6}$ m2		√	
	6/mmm			√
Monoclinic	2	√	√	
	m	√	√	
	2/m			√

Table 2.3 (continued) The 32 crystallographic point groups arranged by crystal systems.

Crystal system	Symbol	Pyroelectric	Piezoelectric	Centro-symmetry
Orthorhombic	222		√	
	mm2	√	√	
	mmm			√
Trigonal	3	√	√	
	$\bar{3}$			√
	32		√	
	3m	√	√	
	$\bar{3}$m			√
Cubic	23		√	
	m3			√
	432			
	$\bar{4}$3m		√	
	m3m			√

A tick (√) indicates the point group is pyroelectric, piezoelectric, or centro-symmetric, as the case may be.

A dielectric material cannot be pyroelectric unless its crystal structure is inherently asymmetric. i.e., it lacks an inversion centre. Of the thirty-two crystal classes, eleven have a centre of symmetry and in another, a combination of symmetries effectively provides a symmetry that endows them with no polar properties. Thus, only twenty classes have an asymmetric structure, and the materials belonging to these classes are piezoelectric which show changes in their internal polarization for changes in mechanical stress and the converse effect also holds. Ten of these twenty classes have a unique polar axis and they posses spontaneous polarization (i.e., electric dipole moment per unit volume) and these materials are pyroelectric (see Table 2.3). A restricted group of the pyroelectrics have the further property of being ferrroelectric,

which has two or more orientation stages (in the absence of an externally impressed electric field), which can be switched from one state to another by an electric field. These two orientational states have identical crystal structure, but differ only in their electric polarization vectors at zero electric field. Thus there are not ferroelectrics, which are not pyroelectric, just as there are not pyroelectrics, which are not piezoelectrics. However, the converse is not true, i.e., all piezoelectrics are not pyroelectric and all pyroelectrics are not ferroelectric, as illustrated in Figure 2.10

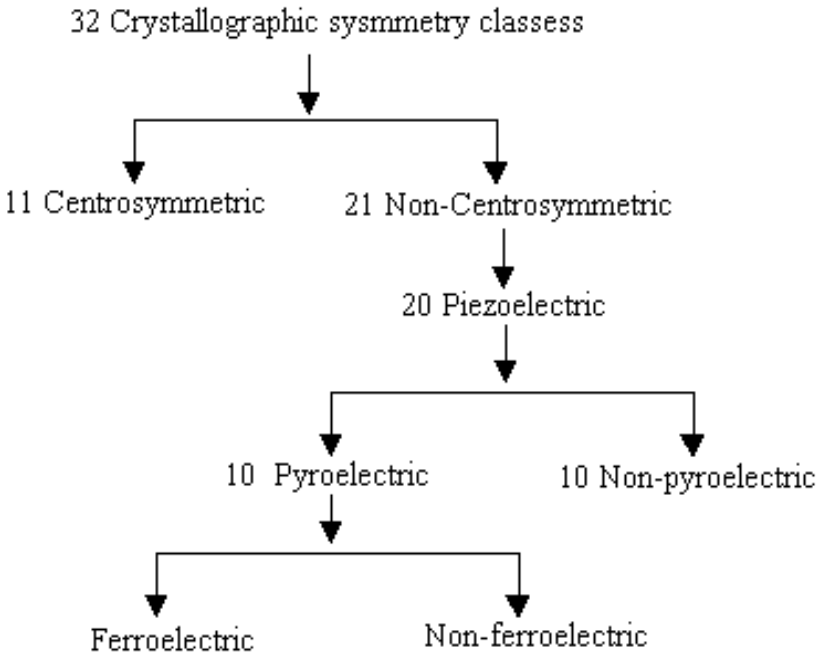

Figure 2.10 Classification of symmetry relating piezoelectric, pyroelectric and ferroelectric materials (Lang and Gupta, 2000)

As the temperature of ferroelectric material increases, its spontaneous polarization decreases and ultimately disappears at the Curie temperature (T_c). The dependence of polarization on the temperature is typically of the form illustrated in Figure 2.11.

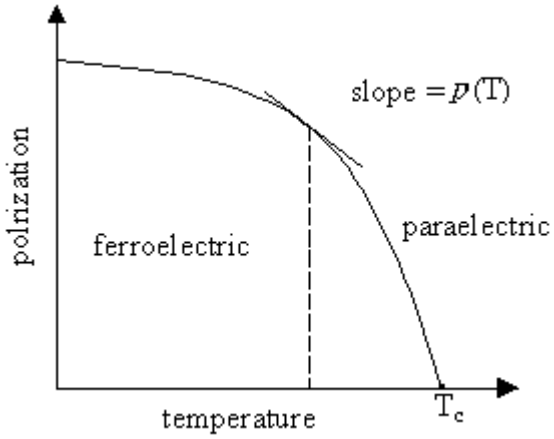

Figure 2.11 The variation in spontaneous polarization with temperature for a ferroelectric material (Limbong, 2000)

From Figure 2.11 the pyroelectric coefficient corresponds to the slope of P versus T. The pyroelectric coefficient was very large as the temperature approaches T_c from below, then becomes zero above T_c.

2.2.1 Inherent and Induced Pyroelectric effects

When the temperature of a pyroelectric material changes, a pyroelectric current is observed. This pyroelectric current results from a change in the spontaneous polarization, caused by the temperature change. If the polarization change is measured without an external field, the effect is referred to as "*inherent pyroelectric effect*"

A relation between the dielectric displacement, the electric field and polarization in a pyroelectric material is defined in equation (2.1). The pyroelectric coefficient is defined formally as changeing the polarization with temperature, at constant field.

$$p = \left(\frac{dD}{dT} \right)_E = \left(\frac{dP}{dT} \right)_E \tag{2.48}$$

The application of a DC electric field to a pyroelectric material results in an increase in the pyroelectric response. The additional response is referred to as "*the induced pyroelectric effect*" The application of the field adds an induced polarization to the polarization which exists at zero field. With the application of an external electric field the total displacement is

$$D(E,T) = D_0(T) + \int_0^E \left(\frac{\partial D}{\partial E} \right) dE' \tag{2.49}$$

where $D_0(T)$ is the displacement at zero field. From $D = \varepsilon_0 E + P_S$, equation (2.49) can be re-written as

$$D(E,T) = P_s(T) + \int_0^E \left(\frac{\partial D}{\partial E} \right) dE' \tag{2.50}$$

$$p = \left(\frac{\partial D(E,T)}{\partial T} \right) \tag{2.51}$$

$$p = \left(\frac{\partial P_s(T)}{\partial T} \right) + \int_0^E \left(\frac{\partial^2 D}{\partial T \partial E} \right) dE' \tag{2.52}$$

$$p = \left(\frac{\partial D}{\partial T} \right)_E = p_{inh.} + \varepsilon_0 \int_0^E \left(\frac{\partial \varepsilon}{\partial T} \right) dE' \tag{2.53}$$

In equation (2.53), $p_{inh.}$ represents the pyroelectric coefficient arising from the ferroelectric polarization at the field *E*. The integral term is the contributions to the pyroelectric effect from the extra induced atomic and electronic polarization at the field *E*.

2.3 Pyroelectric coefficient measurement

When the temperature of a pyroelectric material changes, a current flows in an external circuit connected to the electrodes of the material. This current may have two origins. One component of the current may be the polarization current, while the other is the pyroelectric current. The former is usually observed during the first heating process and is irreversible, while the latter can be observed in both heating and cooling processes and is reversible. Several procedures can be used to measure the pyroelectric coefficient based on direct, dielectric and dynamic methods.

2.3.1 Direct Method

In this work, we use this method to determine the pyroelectric coefficient of the composite sample. Equations (2.54) and (2.55) indicate that the pyroelectric coefficient p can be measured either by measuring the current generated for a known rate of the temperature, or by measuring the charge generated for a known temperature change (Lang and Gupta, 2002)

$$p = \frac{\Delta Q / A}{\Delta T} \tag{2.54}$$

$$p = \frac{I}{A(dT/dt)} \tag{2.55}$$

where A is the sample electrode area and I is the measured pyroelectric current.

2.3.2 Dielectric Heating Method

This method is applicable for polar polymers, such as PVDF, that are dielectrically lossy. In this method, sinusoidal electric field ($E = E_0 sin\ \omega t$) is applied to the sample, causing in the thermal energy is generated, in proportion to the dielectric loss ($tan\delta$). This power is given by

$$U = \varepsilon_0 \varepsilon \omega E_{rms}^2 \tan\delta \tag{2.56}$$

The heating rate is proportional to power dissipation:

$$\frac{dT}{dt} = \frac{U}{C_V} \tag{2.57}$$

Form equation (2.56) and (2.57), equation (2.55) can be rewritten as

$$p = \left(\frac{C_0 C_V}{\varepsilon_0 \varepsilon A \tan\delta} \right) \left(\frac{1}{\omega E_{rms}^2} \right) \frac{dV}{dt} \tag{2.58}$$

where C_0 is the known capacitance across a voltage V, proportional to the polarization developed, $tan\delta$ the loss tangent, ε the dielectric constant and E the sinusoidal electric field. For a known dV/dt, the pyroelectric coefficient can be calculated.

2.3.3 Dynamic method

In this method, a modulated infrared radiation source is used to heat the sample. The pyroelectric coefficient can be written as (Lang and Gupta, 2000)

$$p = \frac{\eta d C_V}{W} \frac{i_p}{f(\omega)} \tag{2.59}$$

where C_v is the volume heat capacity, W is the radiation power, η is the absorbtivity, i_p is the pyroelectric current and $f(\omega)$ is a factor which allows situations where the temperature is not uniformly distributed in the material. At frequencies larger than the inverse of the thermal time constant, $f(\omega)$ =1.

3. Thermal diffusivity and measurements

Thermal diffusivity (α), in heat transfer analysis, is the ratio of thermal conductivity[1] to the heat capacity. Substances with high α will rapidly adjust their temperature to that of surroundings, because they conduct heat quickly in comparison to their thermal 'bulk'.

$$\alpha = \frac{k}{\rho c_p} \tag{2.60}$$

where α is the thermal diffusivity ($m^2 s^{-1}$), k is the thermal conductivity ($W\, m^{-1} K^{-1}$), ρ is density ($kg\, m^{-3}$), and c_p is heat capacity per unit mass ($J\, kg^{-1} K^{-1}$).

Thermal diffusivity is one of the important thermal properties of a solid material. Knowledge of the thermal diffusivity of a pyroelectric material is especially necessary in the design of infrared detectors and detector arrays. The technique for measurement of the thermal diffusivity of the sample based upon periodic heating of one surface of the sample. And then the phase retardation of the thermal wave passing through the sample is obtained.

In practice, the sample is attached by means of cement or solder to a pyroelectric detector, usually $LiTaO_3$. The pyroelectric detector is soldered to a metal plate, which acts as a substrate. A very thin opaque layer is deposited upon the top surface of the sample to improve the laser beam absorption and this is exposed to a laser beam that is intensity-modulated in a sinusoidal fashion by means of an acouto-optic modulator or a light chopper (Figure 2.12).

The laser beam is absorbed by opaque layer of the sample. The sinusoidal modulation of the laser beam causes a sinusoidal fluctuation in temperature of the top

[1]Thermal conductivity is the quantity of heat that passes in unit time through unit area of a plate of unit thickness when its opposite faces differ in temperature by one degree. (SI unit $W\, m^{-1}\, K^{-1}$)

surface of the sample, and this results in the propagation of thermal waves into the sample. The thermal waves are attenuated as they diffuse through the sample and they are also retarded in phase relative to the phase of the laser beam modulation. Thus, a non-uniformly distributed thermal force acts on the sample (Figure 2.13). The phase retardation of the thermal waves in the sample is determined from the pyroelectric current of the detector.

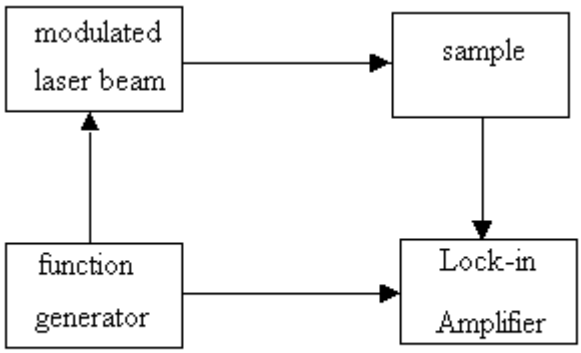

Figure 2.12 Schematic diagram for the measurement of the thermal diffusivity

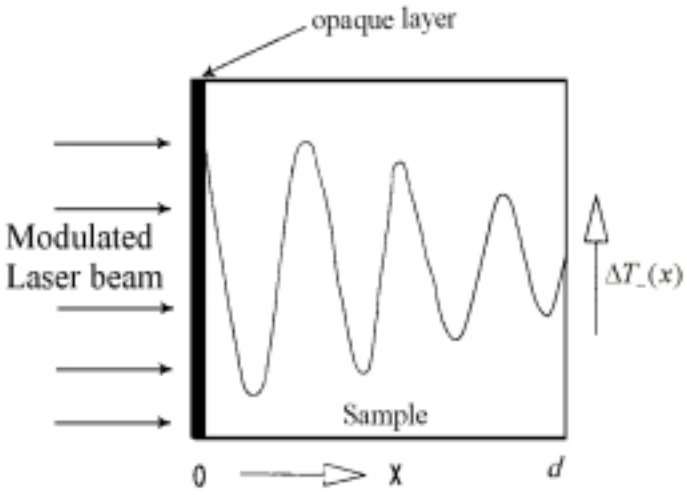

Figure 2.13 Temperature fluctuations inside the sample (Limbong, 2000)

$\Delta T_{\sim}(x)$ is a complex quantity, indicating that the temperature oscillation inside the sample may be phase-shifted with respect to the laser beam. A sample

thickness L, which is illuminated from the $x = 0$ side by a sinusoidally modulated laser beam with a time-dependent laser intensity.

$$j = j_0 + j_{\sim} e^{i\omega t} = j_0 + j_{\sim} e^{i(2\pi f)t}, \tag{2.61}$$

where f is the modulation frequency = $\omega/2\pi$.

The penetration depth of thermal waves is altered by a variation of modulation frequency. The relationship between the penetration depth and modulation frequency is expressed by (Ploss et al., 1992)

$$x_r = \frac{1}{k_r} = \sqrt{\frac{2\alpha}{\omega}} \tag{2.62}$$

x_r = The penetration depth of thermal wave

k_r = The thermal wave vector

α = Thermal diffusivity ($m^2 s^{-1}$)

ω = The radial modulation frequency $=2\pi f$

Figure 2.14 shows how the rate of change of temperature, varies through the sample thickness. The temperature fluctuations penetrate to shallower depths as the frequency of the modulation increased. The highest amplitude is reached near the top surface, while at the rear surface the temperature variation becomes very small.

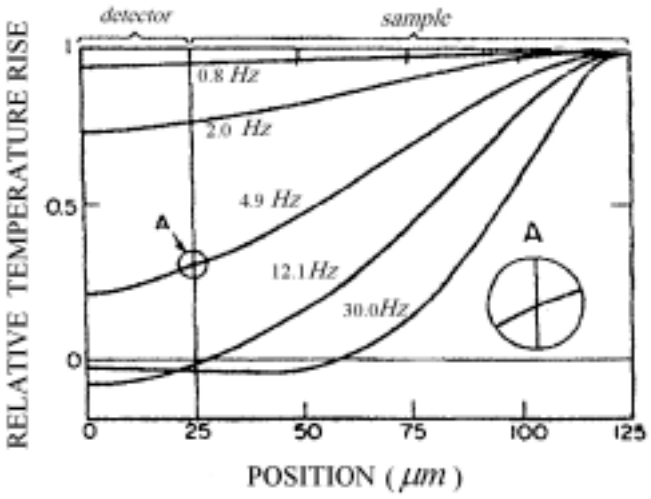

Figure 2.14 Demonstration showing of the temperature different at the frequency at which the surface temperature is a maximum (Lang, 1989).

From Figure 2.14, If the modulation frequency of the laser is small, the whole sample is heated homogeneously. At high frequency the temperature variation at rear surface becomes smaller, and oscillation at different points inside the sample no longer happens synchronously.

The thermal diffusivity of the sample can be obtained by the following analysis:

In the system, there are five layers of the experimental samples. They are composed as follows:

1. Absorption layer, located in the region $z_0 \le z \le z_1$
2. Test sample, located in the region $z_1 \le z \le z_2$
3. Thermally conductive adhesive material, located in the region $z_2 \le z \le z_3$
4. $LiTaO_3$ pyroelectric detector, located in the region $z_3 \le z \le z_4$
5. Brass substrate, located in the region $z_4 \le z \le z_5$

The temperature distribution of each layer is described by the one-dimensional heat conduction equation (equation 2.63)

$$\frac{\partial T_n(x,t)}{\partial t} = \alpha_n \frac{\partial^2 T_n(x,t)}{\partial z^2} \tag{2.63}$$

where T = temperature, t = time, and α_t = thermal diffusivity of layer n. The absorbing layer is exposed to a periodic radiation flux:

$$-k_1 \frac{\partial T(z_0)}{\partial x} = f_0 e^{i\omega t} \tag{2.64}$$

where k_1 is the thermal diffusivity of the top layer, f_0 is the flux intensity of the laser, ω is the radial frequency of laser intensity modulation and i is the imaginary operator. There are two boundary conditions at each surface between two solid layers:

$$T_n = T_{n+1} \tag{2.65}$$

$$k_n \frac{\partial T_n}{\partial z} = k_{n+1} \frac{\partial T_{n+1}}{\partial z} \tag{2.66}$$

The rare surface of the sample has a boundary condition:

$$\frac{\partial T(z_5)}{\partial t} = 0 \tag{2.67}$$

We assume that the temperature varies periodically in time:

$$T(z,t) = e^{i\omega t} u(z) \tag{2.68}$$

From equations (2.68) and (2.64), the differential equation for each layer becomes:

$$\frac{\partial^2 u_n(z)}{\partial z^2} - \frac{i\omega}{\alpha_n} u_n(z) = 0 \tag{2.69}$$

The solution of equation (2.69) is:

$$u_n(z) = a_{1n}\sinh(\kappa_n z) + a_{2n}\cosh(\kappa_n z) \tag{2.70}$$

or $$u_n(z) = a_{1n}e^{\kappa z} + a_{2n}e^{-\kappa z} \tag{2.71}$$

The ten coefficients (a_{1n} *and* a_{2n}) in equation (2.70) are found from the set of transformed boundary conditions by conventional matrix methods.

The pyroelectric current developed in the pyroelectric detector layer is

$$I(t) = pA\left(\frac{du}{dt}\right) \tag{2.72}$$

where A is the cross section area of the laser beam. The phase retardation is found from the real $\Re(I)$ and imaginary parts $\Im(I)$ of the current

$$\theta = \tan^{-1}\left(\frac{\Im(I)}{\Re(I)}\right) \tag{2.73}$$

4. Piezocomposite

A composite material is a materials system composed of a mixture or combination of two or more micro- or macro constituents that differ in form and which are essentially insoluble in each other. Piezocomposite composed of a piezoelectric ceramic and a non-piezoelectric polymer are promising materials because of their excellent tailorable properties.

4.1 Connectivity

The geometry for two-phase composite can be classified according to the connectivity of each phase. The concept of "*connectivity*" for classifying the various composite structures is introduced by Newnham et al. (Newnham, 1987). When

considering a two-phase composite, the connectivity of each phase is identified; e.g., if a phase is self-connected in all x, y and z directions, it is called “3” ,if a phase is self-connected only in z direction, it is called “1”. A diphasic composite is identified with this notation with two numbers m-n, where m stands for the connectivity of an active phase (such as PZT) and n for an inactive phase (such as epoxy resin). In general, there are ten types of diphasic composite: 0-0, 1-0, 2-0, ….., 3-2, 3-3, as illustrated in Figure 2.15 (Uchino, 2000).

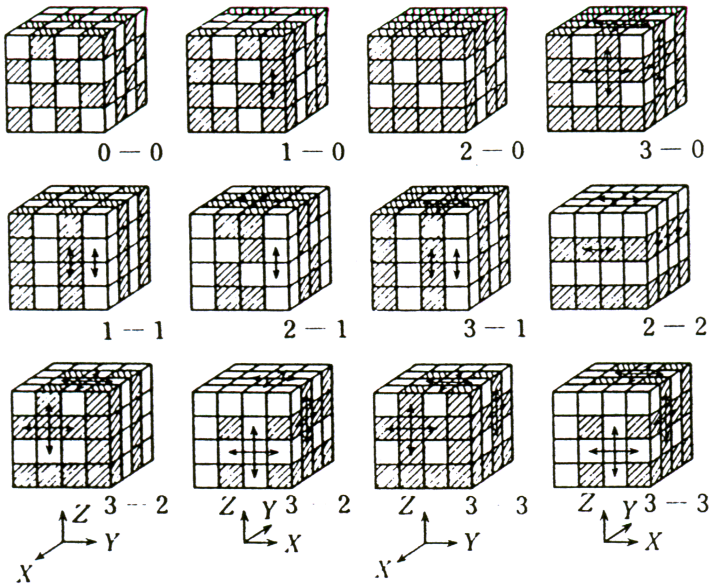

Figure 2.15 Classification of two-phase composites with respect to connectivity (Uchino, 2000)

A variety of new piezoelectric materials can be made by combining a active piezoelectric ceramic with a passive polymer phase. These new piezoelectric materials greatly extend the range of material properties offered by the conventional piezoelectric ceramic and polymer. The most commonly studied composite (also used in this work) are 0-3 and 1-3 configurations and the former one owed its popularity to the easy fabrication procedure which allows for commercial product at a relatively low cost.

4.2 Materials

The samples used in the present work were composites in two connectivities. The firsts were 1-3 composites, which were composed of ceramic (PZT) and epoxy. The seconds were 0-3 composites, which were consisted of ceramic PZT and copolymer (P(VDF-TrFE)). The present section describes detail of composites, together with PZT and copolymer.

4.2.1) 1-3 composite PZT/epoxy

Because the epoxy has no spontaneous polarization, only the PZT rods exhibit the piezo- and pyroelectric phenomenon. Lead zirconate titanate, PZT is a ceramic material used in a variety of memory applications, microphones, transducer, and actuators. PZT is a solid solution phase of lead titanate and lead zirconate. Its chemical formula is $Pb(Zr_xTi_{1-x})O_3$ has the perovskite structure with titanium and zirconium atoms occupying A-sites at random, and lead atom situated at the corners of the unit cell with oxygen atoms located at the surface centers. Figure 2.16 (A) shows perovskite structure of the PZT and Figure 2.16 (B) show the movement of the Ti or Zr atoms under electric fields

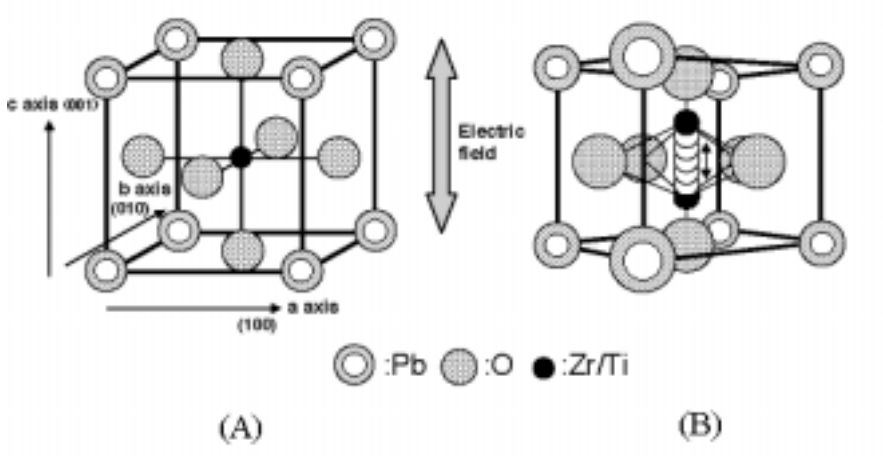

Figure 2.16 Structure of the PZT (A) perovskite structure of the PZT (B) the movement of the Ti or Zr atom under electric fields (Chen, 2001)

PZT has many advantages, as compared to ferroelectric polymer, such as good piezo- and pyroelectric response, high dielectric constant. These properties result in wide applications. However, PZT also have some disadvantages, such as poor mechanical strength. In order to improve the mechanical properties of PZT, it is mixed with other polymers to produce composite materials. Piezocomposite material is an important update of existing piezoelectric ceramic. R. Newnham at the Material Research Laboratory of Pennsylvania State University, USA, has pioneered much of the basic development work. The composite consisting of ceramic rods extending between the major surfaces of a polymer dish has a 1-3 connectivity (Figure 2.17).

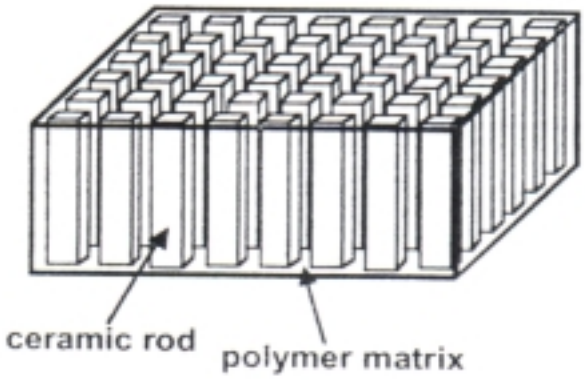

Figure 2.17 Schematic representation of a 1-3 composite PZT/polymer

The advantages of this composite are high electromechanical coupling factors[2], low acoustic impedance, good matching to water or human tissue, and mechanical flexibility (Table 2.4). The thickness-mode electromechanical coupling factor of the composite can be exceed the k_t (0.40-0.50) of the constituent ceramic, approaching almost the value of a rod-mode electromechanical coupling factor, k_{33}

[2] The electromechanical coupling factor, *k,* is the fraction of electrical energy it can convert into mechanical energy and vice verse.

$$k = \sqrt{\frac{mechanical\ energy\ converted\ to\ electrical\ energy}{input\ mechanical\ energy}}$$

or $$k = \sqrt{\frac{electrical\ energy\ converted\ to\ mechanical\ energy}{input\ electrical\ energy}}$$

(0.70-0.80) of that ceramic. The acoustic impedance Z is a parameter used for evaluating the acoustic energy transfer between two materials and defined, in general, by

$$Z = \sqrt{\rho c} \tag{2.74}$$

where ρ is the density and c is the stiffness of the materials. The acoustics matches to the tissue or water (1.5 Mrayls) of the typical piezoceramic (20-30 Mrayls) is significantly improved by forming a composite structure, that is, by replacing some of the heavy, stiff ceramic with a light, soft polymer.

Table 2.4 Typical data of piezoelectric material

Material	1-3 composite	PZT	PVDF, P(VDF-TrFE)
Acoustic Impedance: Z	8-12	30-32	4-5
Thickness coupling factor: k_t	0.45-0.5	0.5-0.7	0.2-0.3
Dielectric constant: ε	200-600	250-2000	6
Density	3.5-4	7.8	2
Maximum temperature(^{0}C)	100	300	80

Piezocomposite materials are especially useful for underwater sonar and medical diagnostic ultrasonic transducer application (see section 4.4)

4.2.2) 0-3 composite PZT/P(VDF-TrFE)

0-3 composites of lead zirconate titanate particles dispersed in a polyvinylidene fluoride-trifluoroethylene copolymer matrix have a good potential for pyroelectric sensor application (Figure 2.18). One particular feature of the composites of PZT particles in poly(vinylidene fluoride-trifluoroethylene) P(VDF-TrFE) copolymer is that the matrix and inclusions can be polarized in parallel or in

antiparallel direction. When the matrix and the inclusions are polarized in opposite directions, the pyroelectric activity will be reduced but the piezoelectric activity reinforced. On the other hand, if the two phases are polarized in parallel, the pyroelectric response reinforces while the piezoelectric activity will be reduced.

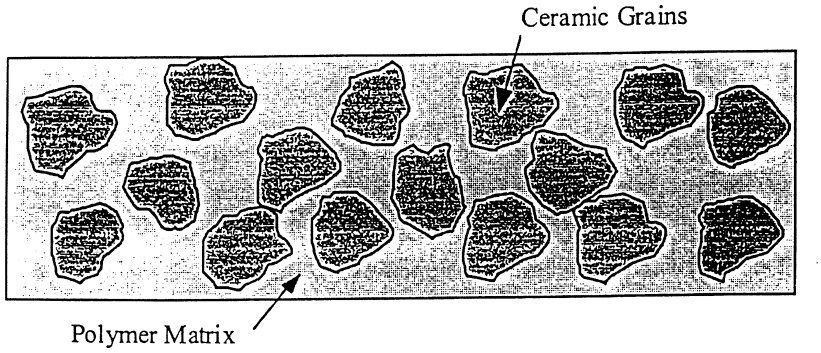

Figure 2.18 Low ceramic volume fraction 0-3 connectivity composite where the ceramic grains are isolated from each other and zero degree connectivity and the polymer is connected to itself with three degrees of connectivity.

The polyvinylidene fluoride: PVDF molecules have a repeat unit of $-CH_2-CF_2-$. PVDF is a semicrystalline polymer. PVDF has at least four polymorphic phases, i.e., $\alpha-, \beta-, \gamma-$ and $\delta-$ phases. The $\beta-$phase of PVDF is probably the most important of the four polymorphics in piezoelectric and pyroelectric applications. Although each of the $\beta-$phase has a dipole moment, because of the random orientation of the crystallites there is no net polarization until it is poled by an application of an external electric field, which encourages a dipolar orientation of it crystallites.

Copolymer of vinylidene fluoride with trifluorothylene P(VDF-TrFE) have all-trans conformation of the $\beta-$phase and exhibit a ferroelectric to paraelectric phase transition at temperatures dependent on content of two monomer constituents. Table 2.5 summarizes the relevant properties of copolymers at varying VDF content. It is generally seen that the pyroelectric coefficient, dielectric constant, loss tangent decrease as the VDF content in the copolymers increases. The Curie temperature, the spontaneous polarization increases with increasing content of VDF.

Table 2.5 Properties of P(VDF-TrFE) copolymers for different VDF fractions (Limbong, 2000)

Composition VDF/TrFE	50/50	56/44	65/35	70/30	75/25	80/20
$p\,(\mu C/m^{-2}\ ^0C)$	40	38	36	35	33	31
ε (at 1 kHz)	18	12	9	8	7.4	7
$\tan\delta$ (at 1 kHz)	0.035	0.025	0.02	0.018	0.017	0.015
$C_V\,(10^6\ Jm^3K^{-1})$	2.3	2.3	2.3	2.3	2.3	2.3
$\delta_t\,(10^{-6}\ m^2s^{-1})$	0.065	0.065	0.065	0.065	0.065	0.065
$T_C\,(^0C)$	45	65	91	106	121	135
$P_s\,(10^4\ Cm^{-2})$	-	7.1	7.9	8.5	9.0	9.4

In the copolymer, the increase of the TrFE fraction produces a decrease in the spontaneous polarization. This is partly due to a decrease in the molecule dipole moment along the 3 direction for the TrFE monomer is haft of that of the VDF monomer. Table 2.6 is a comparison of the material parameters of the ceramic and polymer and the composite.

Table 2.6 Material parameters of the ceramic and polymer compared with those of the composites (Dias and Gupta, 1994).

Material	T_C $(°C)$	T_m $(°C)$	T_g $(°C)$	ε_r	k_t	d_h	g_h	$d_h \times g_h$
Ferroelectric ceramic								
PZT	315			1800	0.48	2.5	40	0.1
$PbTiO_3$	494			230	0.35	23	47	1.08
PTCa	260			213	0.47	61.8	33.6	21
Polymer								
PVDF	205	160	-40	8		-10	-106	1.00
P(VDF-TrFE)	120	180	-30	8-11		-12.6	-170	2.1
PEEK		305	155	3.3				
Epikote		80		3.9				
Ceramic/polymer composite (mixed connectivity 0-3 and 1-3)								
PTCa/P(VDF-TrFE)				51		35	57	2.0
PTCa/Epikote				36		32	72.5	2.32
PTCa/PEEK				19		30	56	1.68

4.3 Theoretical model for composite

The physical properties of composite material, particularly their dielectric, elastic and piezoelectric properties, depend on the properties of the constituent materials, on the relative proportion of these materials and also on geometrical parameters of the microstructure. The basic material parameters of the 1-3 composite are described as following:

- The effective piezoelectric coefficients d^* and g^* of the composite can be interpreted as follows: When an electric field E_3 is applied to this composite, the piezoceramic rods extend easily because the polymer is elastically very soft. Thus, the piezoelectric coefficient of the composite d^* is almost the same as d_{33} of the PZT itself (Uchino, 2000):

$$d_{33}^{*} = d_{33}^{c} \tag{2.75}$$

$$d_{31}^{*} = \phi d_{31}^{c} \tag{2.76}$$

where d_{33}^{*} *and* d_{33}^{c} are the piezoelectric coefficient of the composite and PZT, respectively, ϕ is the volume fraction of the ceramic. On the other hand, during external stress is applied to the composite, the piezoceramic rods will support most of the load, and the effective stress is drastically enhanced and inversely proportional to the volume fraction of ceramic. Thus, larger induced electric fields and large *g** constants are expected:

$$g_{33}^{*} = \frac{d_{33}^{*}}{\varepsilon_0 \varepsilon_{33}^{*}} = \frac{d_{33}}{\phi \varepsilon_0 \varepsilon_{33}} = \frac{g_{33}}{\phi} \tag{2.77}$$

where d_{33}, g_{33} are the piezoelectric coefficient of the PZT. As predicted by the model for this composite, the measured d_{33}^{*} values is independent of ceramic volume fraction, but it is only about 75% of the d_{33} value of PZT. This discrepancy may be due to incomplete poling of the rods. A linear relation between permittivity and the volume fraction of ceramic is almost satisfied, resulting in a dramatic increase in g_{33}^{*} with decreasing fraction of PZT.

- The density ρ^{*} of the composite varies linearly with volume fraction of PZT (Chan, 1989)

$$\rho^{*} = \phi \rho^{c} + (1-\phi)\rho^{p} \tag{2.78}$$

where ρ is the density and superscript *, c, p refer to the composite, ceramic and polymer respectively.

- The dielectric constant of the composite varies essentially linearly with volume fraction of ceramic ϕ. This is because the dielectric constant of the polymer is

small compared to that of the ceramic and its contribution to the overall dielectric constant value is negligible when ceramic volume fraction is high.

- The pyroelectric coefficient p of the composite may be expressed as (Lang and Gupta, 2000),

$$p^* = \phi \xi p^c \tag{2.79}$$

where ξ is the poling ratio, defined as the ratio of an arbitrarily chosen value of polarization to that of saturation polarization at a particular field, p is the pyroelectric coefficient.

4.4 Applications

Piezo- and pyroelectric composites are an important branch of modern materials with wide applications in actuator and sensors in smart materials and structures. Combining two or more distinct constituents piezoelectric composite materials can take the advantages of each constituent and have superior electromechanical coupling characteristics in comparison with homogeneous piezoelectric materials. In this work, we studied the piezo- and pyroelectric and thermal properties of the composite for transducer and detector applications.

4.4.1 Piezoelectric devices

The most widely used commercial piezoelectric material is the various phases of lead zirconate titanate (PZT). Unfortunately, ceramics transducers are fragile and very difficult to produce them in large size. Beyond the enhancement of the quantifiable material properties, piezocomposites offer significant technological advantages for designer of ultrasonic transducer. The higher electromechanical coupling factors and reduced acoustic impedance lead directly to high sensitive and broader bandwidth.

The single-element transducer is base on a piezoelectric plate or disc poled along the thickness direction, the thickness defines the resonance frequency of the device through the equation: thickness = half wavelength (Figure 2.19). When an electrical impulse is applied to the two metallized faces of the plate, an acoustic resonance appears, which will lead to generate the pressure both in the front and back directions. Since the plate, typically a piezoceramic, has high acoustic impedance (i.e. around 33 MRa) compared to biological tissue (close to that of water, i.e. 1.5 MRa), the duration of the acoustic resonance will be very high. Thus piezoelectric plate would lead to a very poor axial resolution. Consequently, piezocomposite are used instead of piezoceramic. Because the acoustic impedance of the piezocomposite match to the tissue or water (1.5 MRa), the piezocomposite would improves axial resolution.

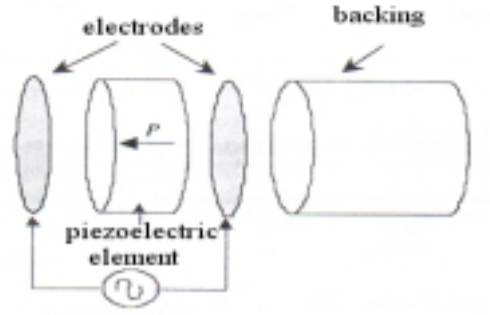

Figure 2.19 Schematic diagram of a classical single-element transducer (Setter, 2002)

Pulse-echo response is obtained by exciting the transducer by an electric impulse of duration less than a period of the active element resonance, and by measuring the echo reflected via a large acoustic mirror immersed in water (Figure 2.20). Radiation patterns can be measured using a point hydrophone receiver which is scanned in the half space in front of the transducer. In transmit/receive mode, a point-target is scanned, and the amplitude of the echo is plotted as function of target position.

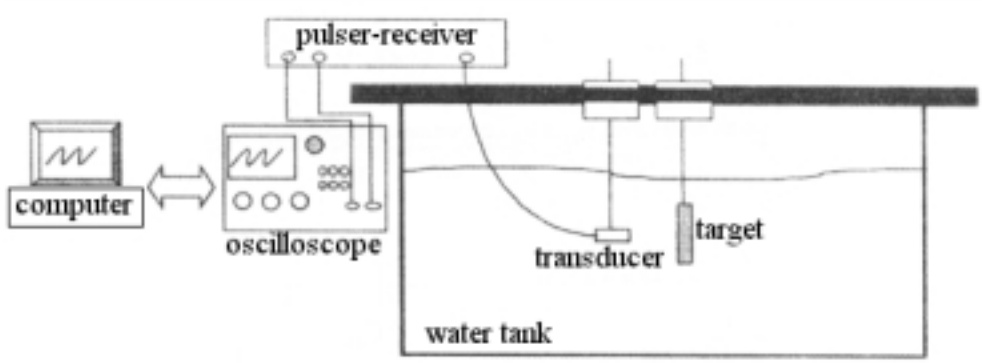

Figure 2.20 Set-up of pulse-echo response (Setter, 2002)

Ultrasonic imaging is based on the phenomenon of the reflection and transmission of sound waves at the interface of two media with different acoustic impedance. When the acoustic waves generated by the transducer encounter an impedance discontinuity, some of energy is reflected back and the remaining is transmitted a head (Figure 2.21). The reflected echo on reaching the transducer generates a voltage that is proportional to the acoustic impedance mismatch at the interface between the tissue. The second wave that is transmitted through the interface serves to defect other impedance discontinuities that may be present at farther distances. The relatively small impedance mismatch between soft tissues allows for the ultrasonic waves to propagate across several interfaces providing imaging capability up to large depth. Figure 2.22 shows the high diagnostic performance that can be achieved with modern ultrasonic imaging systems. Table 2.7 shows the samples of the application of piezoelectric material.

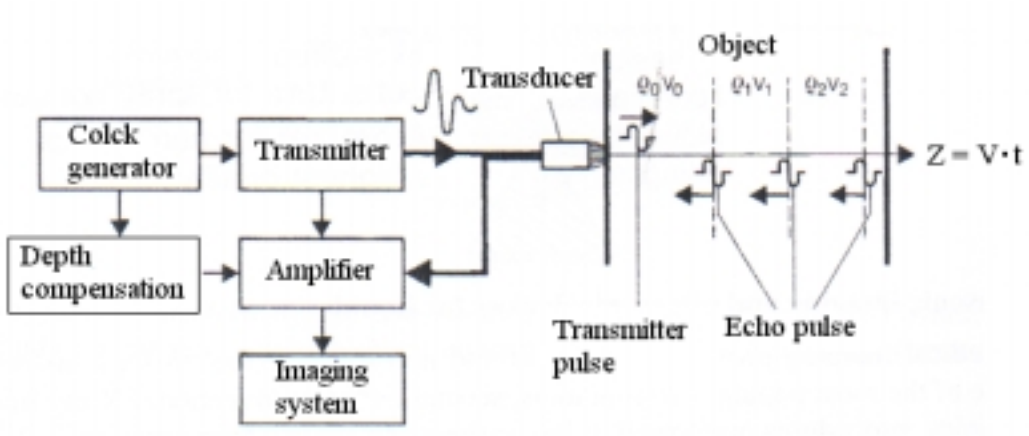

Figure 2.21 Principle of ultrasonic imaging systems (Setter, 2002)

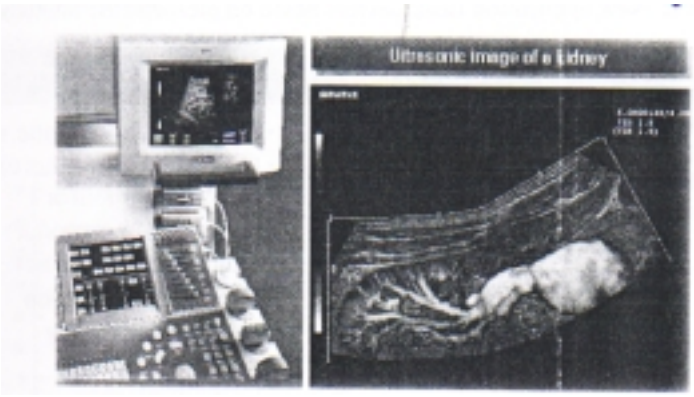

Figure 2.22 Excellence in medical diagnostic achieved with modern ultrasonic imaging (Setter, 2002)

Table 2.7 Examples of the application of the piezoelectric material

Conversion	Application
Mechanical to electrical	- Microphones - Vibration sensors - Accelerometers - Gas igniters
Electrical to mechanical	- Valves - Speaker - Ultrasonic cleaners - Emulsifiers - Sonic transducer

4.4.2 Pyroelectric devices

The detection of long wavelength infrared (IR) radiation is a great interest in a wide range application of pyroelectric effect. Infrared detectors can be roughly classified by their detection principle into quantum or photon detectors and thermal detectors. Quantum detectors are base on the creation of charge carrier (electron-hole pairs) in photoelectric effect of semiconductor materials. These detectors are more sensitive, have fast response time but they suffer from narrow spectral sensitivity. In addition, quantum detectors must operate below or at liquid nitrogen temperatures. This requirement results in adding expensive cryogenic technology. Thermal detector,

convert the energy of IR photon into heat and thus do not require cooling and they are not restricted to use in limited wave-bands as are quantum or photon detectors. There are three types of thermal detectors: microbolometer, pyroelectric and thermocouple detectors. Thermal detectors can operate at room temperature allowing for relatively low cost reliable detection systems in the spectral range of 1-100 μm but they are less sensitive.

The most important type of thermal detector is a pyroelectric one and this is the major area of application for pyroelectric device. Pyroelectric detectors have five main advantages, which make them suitable for many applications.

1. Sensitivity in a very large spectral bandwidth
2. Sensitive in a wide temperature range without need for cooling
3. Low power requirement
4. Fast response
5. Generally low-cost material

Many of the IR detectors utilize a single element. However, there is a great interest in one- and two-dimensional detector arrays, the latter permitting a form of thermal imaging that is analogous to video imaging with visible light. The theories and the use of pyroelectric devices including techniques are described as following.

Infrared radiation exists in the electromagnetic spectrum at a wavelength ($7\times10^{-7} - 1\times10^{-3} m$) that is longer than visible light ($4\times10^{-7} - 7\times10^{-7}$). It can not been seen but it can be detected. Any object, which has a temperature i.e. anything above absolute temperature (0 *K*) radiates in the infrared. The pyroelectric detector is made of a crystalline material that generates a surface electrical charge when exposed to heat in the form of infrared radiation. The charge also change and is measured. Figure 2.23 shows the typical configuration of IR detector.

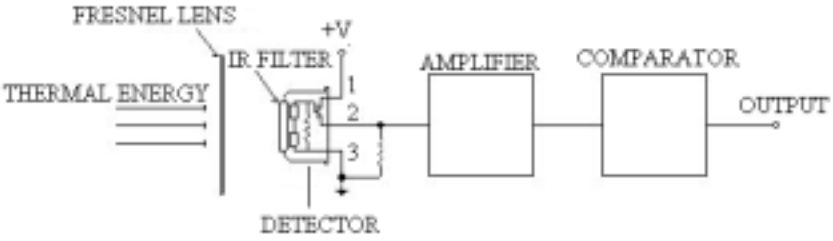

Figure 2.23 Typical configuration of IR detector

A schematic complete design of pyroelectric detector is illustrated in Figure 2.24. A body passing in front of the detector will activate first one and the other element (Figure 2.25).

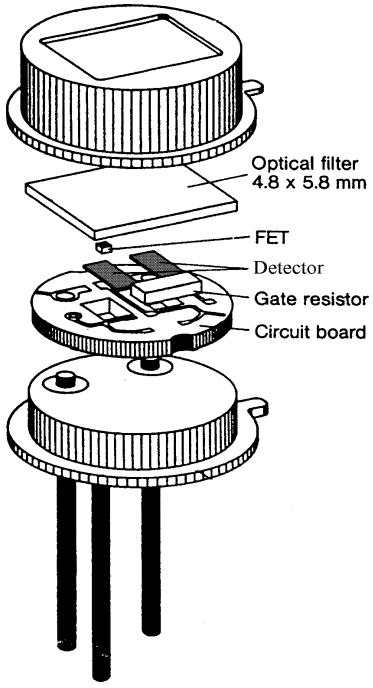

Figure 2.24 Design of a compensated pyroelectric detector (Lang and Gupta, 2000)

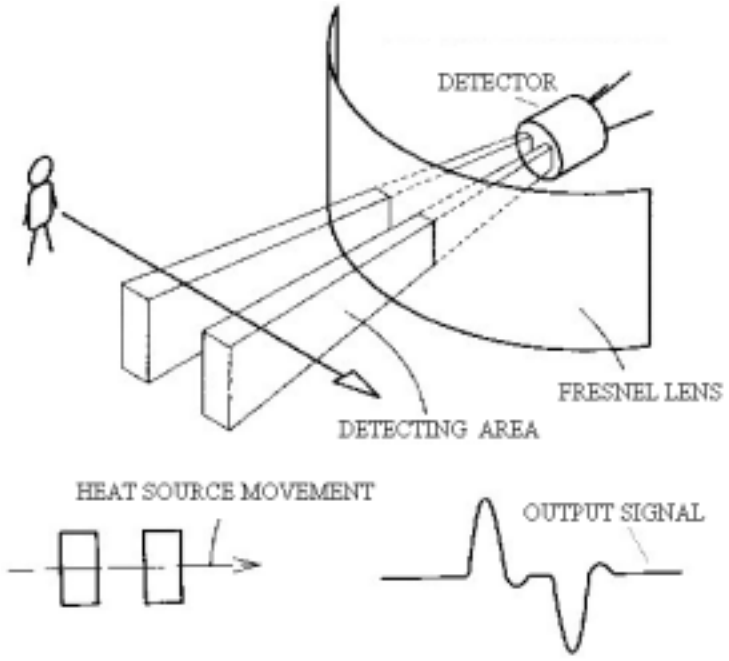

Figure 2.25 Operating of detector

This relatively inexpensive and easy to use pyroelectric detector can be used in a variety of useful devices. Lists of many of the pyroelectric applications are as follows:

Air quality monitoring
Fire alarm
Infrared spectrometer
Pollution detection
Position sensor
Remote sensing
Thermal imaging